



HAL
open science

Solar Refrigeration Based on Impact Ionization in a Transition Metal Dichalcogenides Superlattice

Paul Dalla Valle, Marc Bescond, Fabienne Michelini, Nicolas Cavassilas

► **To cite this version:**

Paul Dalla Valle, Marc Bescond, Fabienne Michelini, Nicolas Cavassilas. Solar Refrigeration Based on Impact Ionization in a Transition Metal Dichalcogenides Superlattice. *Journal of Physical Chemistry C*, 2024, 128 (12), pp.4905-4913. 10.1021/acs.jpcc.3c08273 . hal-04530877

HAL Id: hal-04530877

<https://hal.science/hal-04530877>

Submitted on 3 Apr 2024

HAL is a multi-disciplinary open access archive for the deposit and dissemination of scientific research documents, whether they are published or not. The documents may come from teaching and research institutions in France or abroad, or from public or private research centers.

L'archive ouverte pluridisciplinaire **HAL**, est destinée au dépôt et à la diffusion de documents scientifiques de niveau recherche, publiés ou non, émanant des établissements d'enseignement et de recherche français ou étrangers, des laboratoires publics ou privés.

Solar Refrigeration based on Impact Ionisation in a Transition Metal Dichalcogenides Superlattice

Paul Dalla Valle,^{*,†} Marc Bescond,^{†,‡} Fabienne Michelini,[†] and Nicolas
Cavassilas[†]

[†]*Aix Marseille Université, CNRS, Université de Toulon, IM2NP UMR 7334, 13397,
Marseille, France*

[‡]*Institute of Industrial Science, University of Tokyo, 4-6-1 Komaba, Meguro-ku Tokyo
153-8505, Japan*

E-mail: paul.dalla-valle@im2np.fr

Abstract

Optical refrigeration of a semiconductor generally requires a laser excitation very close to its bandgap and a radiative efficiency close to 1. Under these two conditions, the material can refrigerate by radiating more energy than it absorbs. In this theoretical work, we propose considering impact ionisation, which appears to be predominant in transition metal dichalcogenides, and evaporative cooling to overcome both requirements. With impact ionisation, high-energy photons excite multiple low-energy electron-hole pairs rather than heating the material by emitting phonons when the high-energy carriers thermalise. Thanks to an evaporative cooling effect, such low-energy electron-hole pairs diffuse from a small bandgap absorber into a larger bandgap reservoir by absorbing phonons. This cooling process operates even in materials with modest radiative efficiency. We propose a device based on a small bandgap absorber (a strain-balanced superlattice based on two-dimensional transition metal dichalcogenides) and a larger bandgap reservoir made of bulk MoS₂, forming a type I heterojunction. With a detailed balance approach, parameterised with *ab initio* calculations, we demonstrate a net cooling of the absorber under solar irradiation above 25%, even considering low external radiative efficiency.

Introduction

With the down-scaling of electronic components, the cooling of semiconductors is currently a significant issue in increasing the performance of optoelectronic devices.¹ Optical refrigeration of material uses an incident light source to induce anti-Stokes fluorescence.^{2,3} The photoluminescence must emit photons with higher energy than the incident photons (energy up-conversion) to generate a cooling of the material. During the last two decades, the optical refrigeration of semiconductors has been studied, experimentally and theoretically, in different devices.^{4,5} In particular, it has been investigated in transition metal dichalcogenides (TMD). These materials offer remarkable properties in many optoelectronic applications,

thanks, among other things, to their strong light absorption.^{6,7} The crystal structure of a bulk TMD is a stack of two-dimensional (2D) monolayers. A 2D TMD is an atomic layer of a transition metal (e.g. Mo, W) sandwiched between two atomic layers of chalcogens (e.g. S, Se, Te). The 2D monolayers are bound by van der Waals interactions. By breaking these weak bonds, the 2D TMD can be stacked to form van der Waals heterojunctions (vdWH), offering new properties.^{8,9} In a three-layer heterojunction of TMD (MoSe₂/WS₂/MoS₂), Hao et al. demonstrated an up-conversion of photoluminescence thanks to the ladder band structure of this vdWH.¹⁰ Lai et al. showed that enhancing anti-Stokes scattering (*i.e.* phonon annihilation) over Stokes scattering (*i.e.* phonon generation) was possible in 2D WS₂ thanks to resonant excitation of the anti-Stokes states, leading to Raman cooling.¹¹ A doubly resonant plasmon cavity can improve the energy up-conversion in TMD.¹² Research carried out on optical refrigeration systematically uses a laser as a light source with an energy close to the bandgap, or even below, to generate electron-hole (e-h) pairs with an average energy lower than the thermal energy.¹³ The energy redistribution of the carriers to get a Fermi-Dirac distribution does not emit phonons but absorbs them. Here, we show that considering impact ionisation allows light sources with high-energy photons to be used. Under ideal impact ionisation, when the photon energy is twice the bandgap of the semiconductor, the photogenerated electron scatters with a valence electron and transfers its kinetic energy to induce an additional e-h pair.¹⁴ With this carrier multiplication process, a single high-energy photon generates two e-h pairs of low kinetic energy. This process has been observed experimentally in TMD, where impact ionisation is faster than the phonon emission. Kim et al. and Zheng et al. reported a carrier multiplication efficiency of 99% and 94% respectively in thin films of MoTe₂.^{15,16}

The radiative process causing optical refrigeration generally requires materials with radiative efficiency close to 1.^{17,18} To overcome this requirement and based on the principle of evaporative cooling,¹⁹ we previously showed that extracting the photogenerated carriers into a larger bandgap reservoir generates cooling even with modest radiative efficiencies.²⁰

Such a device requires a type I heterojunction, as shown in Fig. 1. The small bandgap absorber absorbs photons to create e-h pairs with an average energy lower than the large bandgap energy of the reservoir. Once generated, the carriers can either recombine, which is not desired or absorb phonons to be extracted towards the reservoir at higher energy. The phonon absorption induces a heat flux from the absorber into the reservoir.

This theoretical work shows that combining evaporative cooling and impact ionisation can refrigerate the absorber when high-energy photons, particularly sunlight, irradiate the device. We propose a MoS₂/WSe₂ superlattice to form a small bandgap absorber thick enough to absorb the incident light efficiently. The reservoir is a MoS₂ bulk. We have developed a detailed balance model, including impact ionisation, to study the cooling efficiency of our device. We have used *ab initio* calculations to compute the electronic and optical properties of the TMDs.

The article is organised as follows. First, we present the detailed balance model and the device architecture. We show the results, starting with the *ab initio* properties of the superlattice. Then, using our model, we study the cooling efficiency when the device is irradiated by a high-energy laser. Finally, we investigate the performance of the device under sunlight.

Model

This section presents the model based on the detailed balance that simulates optical refrigeration based on evaporative cooling in the presence of impact ionisation. The device is a type I heterojunction shown in Fig. 1. We define $E_{g_{abs}}$ and $E_{g_{res}}$, the bandgap energy of the absorber and the reservoir, respectively. We impose a Fermi-Dirac distribution of the electron populations in the absorber and the reservoir. It assumes that the carrier-carrier interactions induce an instantaneous thermalisation of electrons in conduction bands and holes in valence bands.²¹ Since e-h pair are generated in the absorber, electrons and holes are not

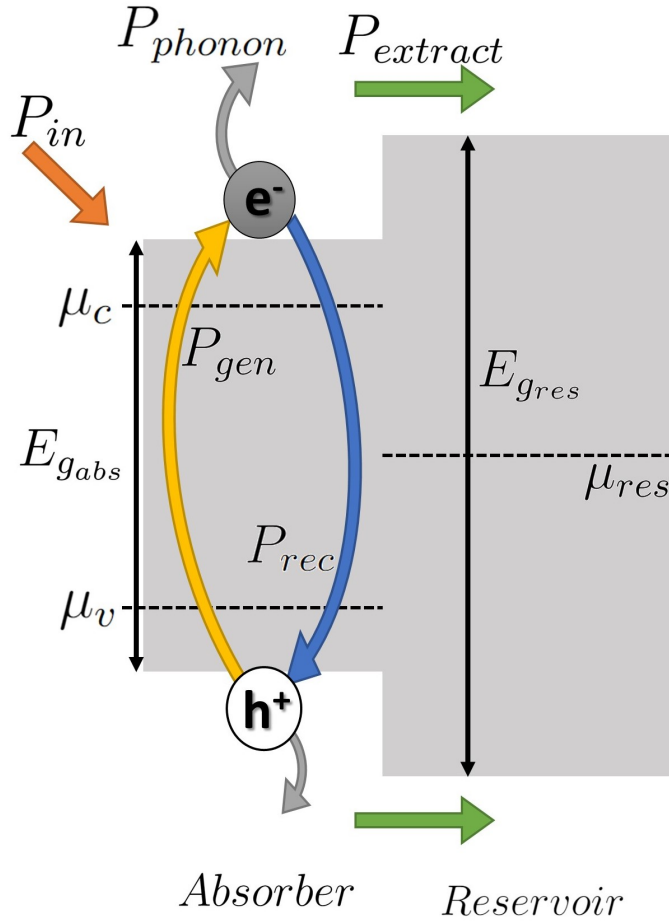


Figure 1: Schematic representation of a cooling device based on a type I heterojunction. Carriers are photogenerated in a small bandgap absorber and obey a Fermi-Dirac distribution with temperature T_c and Fermi level splitting $\Delta\mu = \mu_c - \mu_v$. The photogenerated carriers absorb phonons to be extracted towards a larger bandgap reservoir. The latter is considered infinite, and its electronic distribution is given by a Fermi-Dirac distribution with $T = T_{amb} = 300$ K, electrons and holes in the conduction and valence bands, respectively, share the same Fermi level: μ_{res} . The arrows depict the power flux densities P_{in} is the incident power flux density of the light source, P_{gen} is the power flux density generated through photon absorption, P_{rec} is the power flux density of the carrier recombination, P_{phonon} is the thermal power flux density absorbed by the carriers and $P_{extract}$ is the power flux density diffusing into the reservoir.

in equilibrium with each other, nor with phonons. We define two pseudo-Fermi levels μ_c and μ_v for the electrons in the conduction band and the holes in the valence band, respectively, and we define the carrier temperature in the absorber, T_c , considered equal for electrons and holes. The Fermi-Dirac distribution in the absorber is characterised by T_c (which can differ

from room temperature) and a Fermi level splitting $\Delta\mu = \mu_c - \mu_v$. We consider an infinite reservoir so it can provide or accept carriers without modifying its electronic distribution. The latter is, therefore, a Fermi-Dirac one at room temperature ($T_{amb} = 300$ K) and with a zero Fermi level splitting (*i.e.* electrons and holes are at equilibrium and share the same Fermi level μ_{res}). In our model, the crystal and phonon temperatures in the absorber are constant and equal to room temperature. Such a consideration implies an ideal heat dissipation between the absorber and the environment. Since T_c differs from room temperature, there is an energy exchange between the electronic and phononic baths, characterised by heat exchange in the absorber. In hot-carrier solar cells made of 2D quantum wells, experimental results have shown that the power flux density exchanged between the two baths (P_{phonon}) can be considered proportional to their temperature difference:²²

$$P_{phonon}(T_c) = Q(T_c - T_{amb}), \quad (1)$$

where Q , the thermalisation coefficient, is a specific material parameter. We consider this equation to be true for TMD. This coefficient is related to the electron-phonon scattering and a low value corresponds to a weak electron-phonon interaction. Since Q is positive, if $T_c > 300$ K, P_{phonon} is positive and represents a phonon generation in the material. If $T_c < 300$ K, P_{phonon} is negative, phonon absorption is predominant.

Impact ionisation results in the generation of multiple e-h pairs following the absorption of one high-energy photon. To model this phenomenon, we introduce the quantum yield (QY) function.¹⁴ It defines the number of e-h pairs induced by the absorption of one photon of energy E . $QY(E) = 0$ when $E < E_{g_{abs}}$ since no photon is absorbed. Without impact ionisation, we impose $QY(E) = 1$ when $E \geq E_{g_{abs}}$, *i.e.* one absorbed photon induces one e-h. With ideal impact ionisation, $QY(E) = n$, when $E \in [n \times E_{g_{abs}}, (n + 1) \times E_{g_{abs}}[$, with n an integer. With this energy E , one absorbed photon generates n e-h pairs.

Within the detailed balance approach, we define the carrier generation flux in the absorber

by

$$\begin{cases} J_{gen} = \int_{E_{gabs}}^{\infty} QY(E)\phi_{in}(E)A(E)dE \\ P_{gen} = \int_{E_{gabs}}^{\infty} E\phi_{in}(E)A(E)dE \end{cases}, \quad (2)$$

where J_{gen} is the photogenerated carrier flux and P_{gen} is the associated power flux density. The ϕ_{in} function is the light source's emission spectrum. In the following, we will use either a laser or sunlight. A is the absorbance of the absorber, defined by

$$A(E) = 1 - e^{\alpha(E)L}, \quad (3)$$

where α is the absorption coefficient of the absorber and L is its thickness. In this work, we compute the absorption coefficient by using *ab initio* calculations. Impact ionisation is an elastic phenomenon, so the power flux density induced by the absorption of the incident light (P_{gen}) does not depend on QY. While impact ionisation increases the number of photo-generated particles, the total energy remains constant. Once absorbed, the carriers can recombine directly in the absorber or be extracted to the reservoir. The total recombination of carriers in the absorber is given by

$$\begin{cases} J_{rec}(\Delta\mu, T_c) = \frac{1}{\eta_{rad}} \int_{E_{gabs}}^{\infty} QY(E)4n_{op}^2 L\alpha(E)\phi_{BB}(E)e^{\frac{\eta_c(T_c)E}{k_B T_{amb}}} e^{-\frac{(1-\eta_c(T_c))\Delta\mu QY(E)}{k_B T_{amb}}} dE \\ P_{rec}(\Delta\mu, T_c) = \frac{1}{\eta_{rad}} \int_{E_{gabs}}^{\infty} E4n_{op}^2 L\alpha(E)\phi_{BB}(E)e^{\frac{\eta_c(T_c)E}{k_B T_{amb}}} e^{-\frac{(1-\eta_c(T_c))\Delta\mu}{k_B T_{amb}}} dE \end{cases}, \quad (4)$$

where J_{rec} is the flux and P_{rec} is the associated power flux density of carriers lost by radiative or non-radiative recombination. The derivation of these expressions is shown in Supporting Information. n_{op} is the refractive index of the absorber, ϕ_{BB} is the blackbody radiation at room temperature (T_{amb}),

$$\phi_{BB}(E) = \frac{2\pi}{h^3 c^2} \frac{E^2}{\exp\left(\frac{E}{k_B T_{amb}}\right) - 1}, \quad (5)$$

where h is Planck's constant, c is the speed of light in vacuum, k_B is Boltzmann's constant. In Eq. 4,

$$\eta_c(T_c) = 1 - \frac{T_{amb}}{T_c} \quad (6)$$

is the Carnot's efficiency of the designed cooling device. In Eq. 4, we introduce the external radiative efficiency coefficient (η_{rad}) to include non-radiative recombinations. η_{rad} is the ratio between the radiative recombination rate and the total recombination rate.²³ It is important to include non-radiative recombination in our model since such a process may reduce the cooling efficiency and may also generate phonon in the absorber, which could heat up the later. J_{rec} depends on QY because impact ionisation induces more photogenerated carriers and, thus, more recombinations. Consequently, the chemical potential of the emitted photons equals $\Delta\mu \times \text{QY}$, which is required by thermodynamics.²⁴ Again, since the phenomenon is elastic, impact ionisation does not affect P_{rec} . We define the flux of carriers extracted from the absorber to the reservoir and the corresponding power flux density by

$$\begin{cases} J_{extract}(\Delta\mu, T_c) = \int_{E_{gres}}^{\infty} \frac{8\pi m^*}{h^3} (E - E_{gres}) \left(\frac{1}{1 + \exp\left(\frac{(1-\eta_c(T_c))(E-\Delta\mu)}{2k_B T_{amb}}\right)} - \frac{1}{1 + \exp\left(\frac{E}{2k_B T_{amb}}\right)} \right) dE \\ P_{extract}(\Delta\mu, T_c) = \int_{E_{gres}}^{\infty} \frac{8\pi m^*}{h^3} (E - E_{gres}) E \left(\frac{1}{1 + \exp\left(\frac{(1-\eta_c(T_c))(E-\Delta\mu)}{2k_B T_{amb}}\right)} - \frac{1}{1 + \exp\left(\frac{E}{2k_B T_{amb}}\right)} \right) dE \end{cases} \quad (7)$$

These expressions are based on a three-dimensional (3D) description of the Landauer approach and use the 3D density-of-states in the reservoirs and the effective mass (m^*) approximation. They have been derived in a previous work.²⁰ As $J_{contact}$ and $P_{contact}$ are proportional to m^* , we use the limiting (smallest) effective mass for the implementation. Figure 1 schematically showed the power flux densities in the device. The detailed balance approach imposes a conservation of these fluxes and requires

$$\begin{cases} J_{gen} = J_{rec}(\Delta\mu, T_c) + J_{extract}(\Delta\mu, T_c) \\ P_{gen} = P_{rec}(\Delta\mu, T_c) + P_{extract}(\Delta\mu, T_c) + P_{phonon}(T_c) \end{cases} \quad (8)$$

We solve these equations to find T_c and $\Delta\mu$ and thus the thermodynamic parameters of the electronic distribution in the absorber. We define the cooling efficiency $\eta_{cooling}$ as the ratio between the cooling power flux in the absorber and P_{in} , the incident power flux of the light source. The cooling power flux is the difference between the phonons consumed by the energy exchange between the phononic and electronic baths (*i.e.* $-P_{phonon}$) and the phonons emitted by non-radiative recombination in the absorber (*i.e.* $(1 - \eta_{rad}) \cdot P_{rec}$). Thus,

$$\eta_{cooling} = \frac{-P_{phonon} - (1 - \eta_{rad}) \cdot P_{rec}}{P_{in}} \quad (9)$$

and P_{in} is given by

$$P_{in} = \int_0^{\infty} E \phi_{in}(E) dE. \quad (10)$$

The absorber is cooled when $\eta_{cooling} > 0$. Conversely, when $\eta_{cooling} < 0$, there is a heating.

DFT Methods

The *ab initio* calculations are developed in the framework of plane-wave density functional theory implemented in the Quantum ESPRESSO package.^{25,26} We use the generalised gradient approximation (GGA) of Perdew, Burke and Ernzerhof (PBE) to implement the exchange-correlation functional.²⁷ The van der Waals interactions are included with the Grimme D3 correction.²⁸ The electron-ion interaction is described with normed-conservative pseudopotentials produced using the code ONCVSP (Optimized Norm-Conserving Vanderbilt PseudoPotentials)²⁹ from pseudo-dojo.org.³⁰ The energy cutoff in the calculations is set to be 800 eV, and the total energy is converged to better than 10^{-6} eV. The Hellmann-Feynman forces are converged to less than $2.5 \cdot 10^{-4}$ eV/Å to get the relaxed structures. The Brillouin-Zone is sampled with a (12x12x4) and a (12x12x1) Monkhorste-Park mesh³¹ for bulk and slab calculations respectively. To calculate the absorption coefficient, we used the

post-processing code `epsilon.x` from Quantum ESPRESSO. This code provides the real and imaginary parts of the dielectric tensor from DFT eigenvalues and eigenvectors.

Results and discussions

Ab initio properties of the absorber

The absorber must meet two conditions to obtain an efficient cooling device. It must efficiently absorb the incident photons and must have a small bandgap to enhance the impact ionisation phenomenon since the QY will be higher for a given photon energy if the material's bandgap is smaller. In a previous study, we showed that a 2D MoS₂/WSe₂ vdWH is a type II heterojunction and has a smaller bandgap (0.6 eV) than isolated 2D MoS₂ (1.5 eV) or isolated 2D WSe₂ (1.9 eV).³² Knowing that impact ionisation prevails in TMD,^{15,16} this heterojunction could be a good absorber. However, since 2D TMD layers absorb only 5 to 10% of the incident light,³³ the 2D vdWH is too thin. This is why we propose stacking several periods of this 2D MoS₂/WSe₂ vdWH. In this section, we show that such a superlattice is particularly adapted to impact ionisation due to its small bandgap and, at the same time, offers a large absorption of high-energy photons. We use the framework of density functional theory (DFT) with Quantum Espresso to compute its relaxed crystal structure and its *ab initio* band structure, absorption coefficient and projected charge density (see DFT methods). In DFT, the superlattice is simulated as an infinite repetition of the 2D vdWH along the out-of-plane direction. We impose that the transition metal of MoS₂ (WSe₂) is aligned with the chalcogens of WSe₂ (MoS₂). This stacking is possible thanks to the moderate difference between the lattice parameter of isolated 2D MoS₂ and isolated 2D WSe₂.^{34,35} In this way, only six atoms compose the unit cell of the superlattice. Its crystal structure is shown in Fig. 2. After optimising and relaxing the crystal structures, the lattice parameters of the isolated 2D MoS₂, isolated 2D WSe₂ and superlattice are 3.185 Å, 3.321 Å and 3.232 Å respectively. In the superlattice, MoS₂ is stretched, and WSe₂ is compressed compared to their

isolated counterparts. The lattice parameter of the superlattice is lower than the average lattice parameter of the isolated 2D MoS₂ and isolated 2D WSe₂ since Young's modulus of WSe₂ is about two-thirds of Young's modulus of MoS₂,³⁶ making WSe₂ more deformable. By construction, the superlattice is a zero average in-plane stress crystal. Such strain-balanced structure suggests that the critical stack thickness can be very large.³⁷

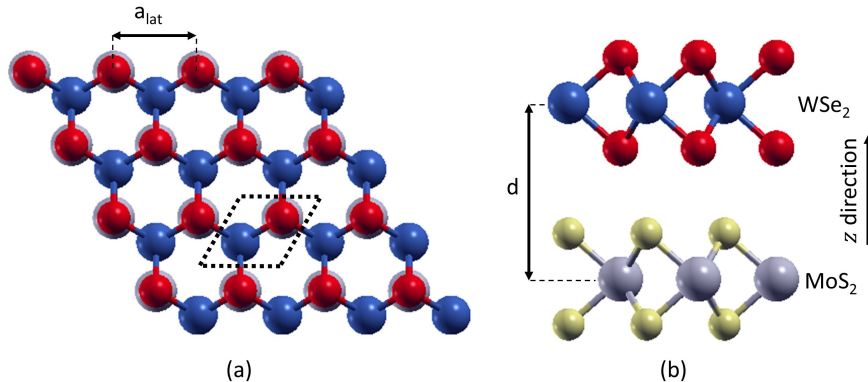


Figure 2: (a) Top and (b) side views of the superlattice crystal structure. The Mo, S, W and Se atoms are represented by grey, yellow, blue and red spheres, respectively. In (a), the black dotted diamond highlights the unit cell. a_{lat} is the relaxed lattice parameter of the heterojunction and d is the interlayer distance between the 2D TMD. The unit cell is repeated ad infinitum along the z direction.

The band structure of the superlattice along $\Gamma - M - K - \Gamma$ path of the first Brillouin zone (Fig. 3(a)) shows a direct bandgap of 0.6 eV at K point. The bandgap energy of the superlattice is equal to the bandgap energy of the 2D MoS₂/WSe₂ vdWH (computed in a previous work³⁸). The absorption coefficient α is computed versus the photon energy E and shown in Fig. 3(b). We impose $\alpha(E) = 0 \text{ cm}^{-1}$ when $E < 0.6 \text{ eV}$ since we assume no absorption below the bandgap of the superlattice. The absorption of the high-energy photons of the solar spectra ($2.5 < E < 4 \text{ eV}$) is efficient, and $\alpha(E) > 6.10^5 \text{ cm}^{-1}$ (which is about one order of magnitude higher than the absorption coefficient of GaAs in this energy range³⁹). When $0.6 < E < 1 \text{ eV}$, $\alpha(E) < 3.10^3 \text{ cm}^{-1}$ (see inset of Fig. 3(b)). So, even though the bandgap is direct and equals 0.6 eV, the absorption of low-energy photons is very weak. To explain this weak absorption, we compute the projected charge density at

K_{VB} (Fig. 3(c)) and K_{CB} (Fig. 3(d)), the valence band edge and the conduction band edge at K point, respectively (see black circles in Fig. 3(a)). The charge density at K_{VB} is localised in WSe₂ principally, while at K_{CB} , the density is localised in MoS₂ principally. At K point, the valence band maximum and the conduction band minimum are not in the same TMD. So, the overlap of the wavefunctions is negligible, and processes that require wave vector conservation, such as photon absorption, are expected to be weak close to the bandgap. This observation is at the origin of the weak absorption of low-energy photons (with $0.6 < E < 1.5$ eV). Finally, we plot the charge density at Γ_{VB} , the valence band edge at Γ point (Fig. 3(e)). The charge density is delocalised in both MoS₂ and WSe₂. Thus, between K_{CB} and Γ_{VB} , we expect strong absorption and emission for processes that do not require wave vector conservation, such as impact ionisation which is an Umklapp scattering.⁴⁰ In the superlattice, knowing that the energy difference between K_{CB} and Γ_{VB} is only 0.62 eV, a photon of energy $E = 1.24$ eV (*i.e.* twice this energy difference) may induce two low-energy e-h pairs close to the band edges thanks to impact ionisation. The superlattice, based on a multiple repetition of 2D MoS₂ and 2D WSe₂, is a material offering an extremely large absorption of high-energy photons and where impact ionisation is expected to be intense.

Cooling efficiency under a high-energy laser

We evaluate the cooling efficiency of the device presented in Fig. 1. The absorber is a 50 nm-thick superlattice ($E_{g_{abs}} = 0.6$ eV), and the reservoir is a bulk of MoS₂. Its bandgap, computed in DFT, is $E_{g_{res}} = 1.0$ eV, and the limiting effective mass is $m^* = 0.3m_0$ (with m_0 the free electron mass). In this section, the light source is a laser that generates photons with an energy between $4 \times E_{g_{abs}}$ and $4 \times E_{g_{abs}} + 40$ meV (in Eq. 2, ϕ_{in} is implemented with a box-car function). In this energy range, the superlattice absorbs 85% of the incident photons (from Eq. 3, with $L = 50$ nm, $A(E) = 85\%$) and $QY(E) = 4$, which highlights the effect of impact ionisation. Figure 4(a) shows the cooling efficiency as a function of the laser power, considering an ideal impact ionisation (blue curve) and without impact ionisation (red

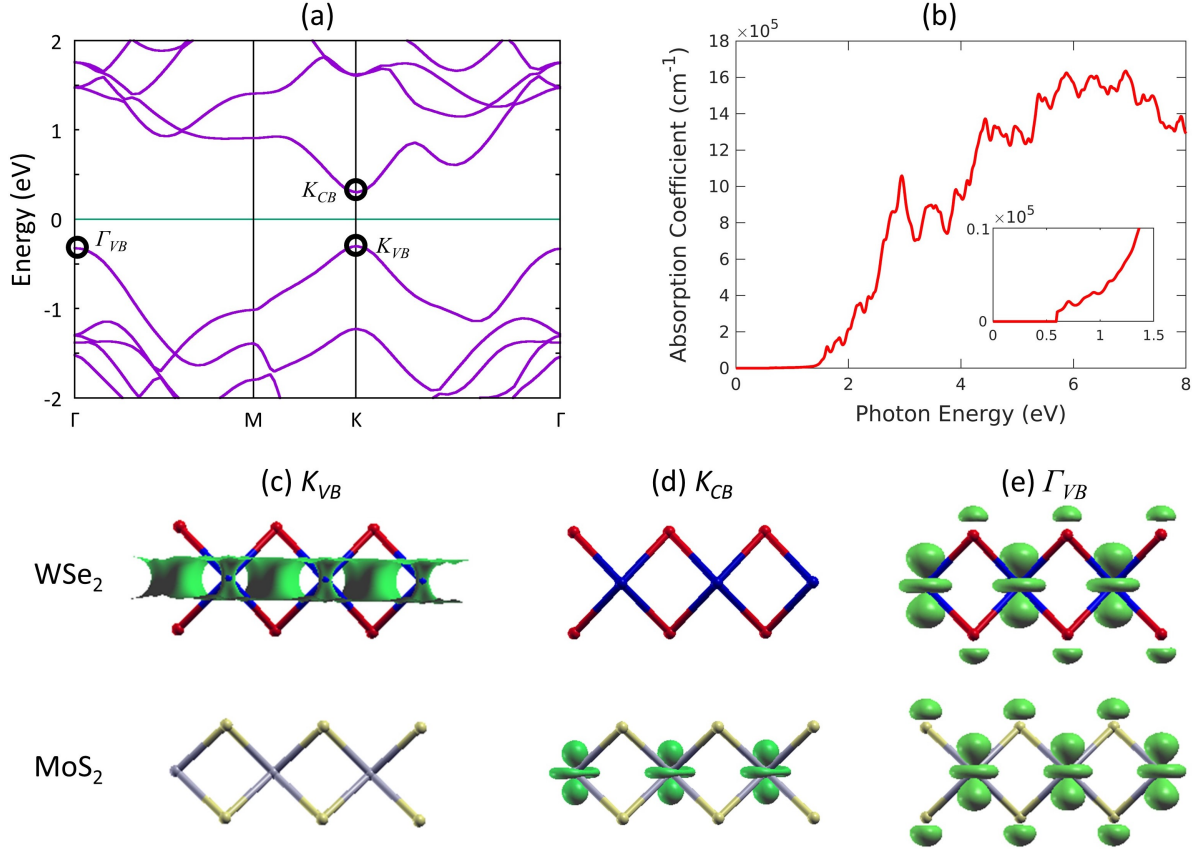


Figure 3: (a) Band structure of the superlattice along the $\Gamma - M - K - \Gamma$ points of the first Brillouin zone. The energy reference is set to the middle of the bandgap. (b) Absorption coefficient α of the superlattice versus the photon energy E . The inset plot is a zoom on the low energy photon ($E < 1.5$ eV). (c), (d) and (e) show the isoline projected charge densities (green shapes) in the superlattice at the band edges K_{VB} , K_{CB} and Γ_{VB} respectively (see (a) for the nomenclature). The Mo, S, W and Se atoms are represented by grey, yellow, blue and red spheres, respectively.

curve). The superlattice's radiative efficiency and thermalisation coefficient are unknown and must be fixed. We set $\eta_{rad} = 10^{-2}$, corresponding to a material with high radiative performance.²³ The thermalisation coefficient is related to the electron-phonon interaction in the material and has been determined experimentally in GaAs multiple quantum wells ($Q_0 = 2.10^5 \text{ W.m}^{-2}.\text{K}^{-1}$).²² The scattering time constant of GaAs and TMD being of the same order of magnitude,¹⁵ we set $Q = Q_0$. We will later examine the impact of these two parameters (η_{rad} and Q) on the cooling efficiency. Without impact ionisation, the efficiency is below zero regardless of the laser power, and the laser heats the absorber (see

Fig. 4(a), red curve). Indeed, the electrons are generated at high energy and thermalise in the absorber by emitting phonons. On the other hand, we observe a positive efficiency with ideal impact ionisation when the laser power is lower than $5 \cdot 10^6 \text{ mW.cm}^{-2}$ (see Fig. 4(a), blue curve), which corresponds to a cooling of the absorber. Electrons generated at high energy elastically transfer the excess energy to valence electrons to create new e-h pairs. When the laser power is lower than 10^5 mW.cm^{-2} , the cooling efficiency of the device is constant, equal to 62%. Increasing the laser power enhances the flux of photogenerated carriers. At constant efficiency, increasing the power of the laser enables the extraction of more heat from the absorber. For laser powers higher than 10^5 mW.cm^{-2} , the efficiency decreases until it becomes negative beyond $5 \cdot 10^6 \text{ mW.cm}^{-2}$. To explain the behaviour, Fig. 4(b) shows the carrier temperature T_c in the absorber versus the laser power, and Fig. 4(c) shows the ratios J_{rec}/J_{gen} and $J_{extract}/J_{gen}$ versus the laser power. For laser powers lower than 10^6 mW.cm^{-2} , the carrier temperature is lower than the ambient temperature and decreases as the power increases (Fig. 4(b)). In this range, the carrier recombination is negligible ($J_{rec}/J_{gen} = 0$), and all the generated carriers are extracted to the reservoir ($J_{extract}/J_{gen} = 1$), see Fig. 4(c). The generated carrier flux is equal to the extracted carrier flux, which increases with the power of the laser. This increase enables more heat extraction and gradually decreases the carrier temperature in the absorber. For laser powers higher than 10^6 mW.cm^{-2} , the generated carrier flux is such that the extraction becomes a limiting factor ($J_{extract}/J_{gen} < 1$). The carrier recombination increases and has two detrimental consequences on the cooling efficiency. First, those carriers are not extracted and do not participate in the cooling. Second, non-radiative recombination induces absorber heating by phonon emission (see Eq. 9). The carrier temperature reaches a minimum and then increases until it becomes higher than the ambient temperature when the laser power exceeds $5 \cdot 10^6 \text{ mW.cm}^{-2}$. Above this value, the recombination is such that the heating by non-radiative recombination exceeds the cooling by carrier extraction. The cooling efficiency becomes negative.

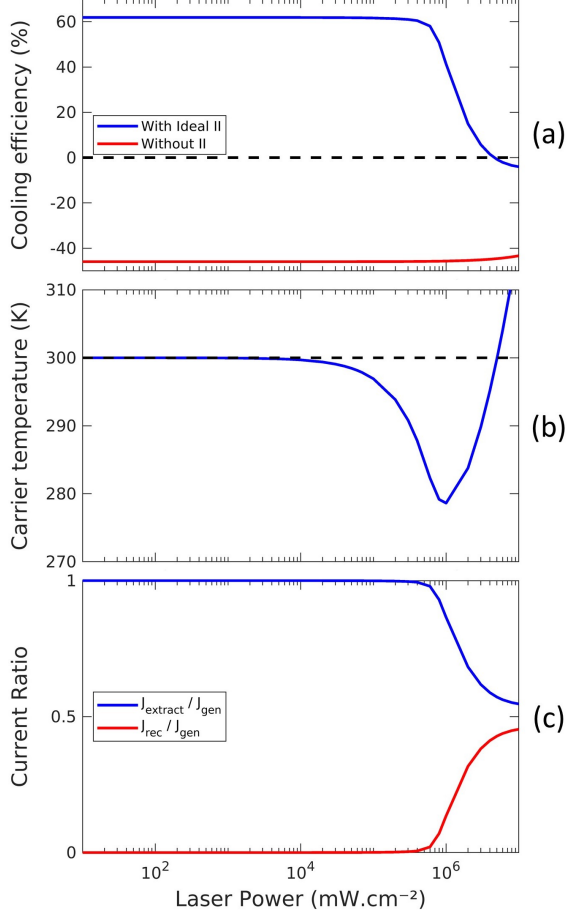


Figure 4: (a) Cooling efficiency $\eta_{cooling}$ with ideal (blue curve) and without (red curve) impact ionisation, (b) carrier temperature T_c and (c) carrier flux ratios J_{rec}/J_{gen} (red curve) and $J_{extract}/J_{gen}$ (blue curve) versus the laser power. The laser generates photons with energy between $4 \times E_{g_{abs}}$ and $4 \times E_{g_{abs}} + 40$ meV, $\eta_{rad} = 10^{-2}$ and $Q = 2.10^5 \text{ W.m}^{-2}.\text{K}^{-1}$.

Cooling efficiency under solar irradiation

Finally, we explore the performance of the device under solar irradiation. The latter is implemented with the blackbody spectrum at temperature $T_{sun} = 5800$ K. So

$$\phi_{in}(E) = C \frac{2\pi}{h^3 c^2} \frac{E^2}{\exp\left(\frac{E}{k_B T_{sun}}\right) - 1} \Omega_{sun}, \quad (11)$$

where C is the concentration factor, and $\Omega_{sun} = 2.153 \times 10^{-5}$ sr is the solid angle of the sunlight on earth. The 50 nm-thick superlattice absorbs 45% of the incident power flux.

The cooling efficiency is computed versus the radiative efficiency and the thermalisation coefficient for different concentrations of the solar flux. In Fig. 5(a), 5(b) and 5(c), the concentration factor is $C = 1$, $C = 10^2$ and $C = 10^4$, respectively. The radiative efficiency varies from 10^{-6} to $3 \cdot 10^{-2}$, corresponding to the radiative quality of Earth-abundant and high-performance materials, respectively.⁴¹ The thermalisation coefficient establishes a linear relationship between the power flux density exchanged with the phonons and the difference between the carrier and crystal temperatures (see Eq. 1). Since the linear behaviour has not been evidenced for TMD and since no experimental values have been measured, we vary this parameter by six orders of magnitude around the experimental value Q_0 . Whatever the solar flux concentration factor, the maximum cooling efficiency achieved by the device is 28%. Without concentration (Fig. 5(a)), this maximum is reached as soon as the radiative efficiency is higher than $5 \cdot 10^{-6}$. Below this value, the cooling efficiency is limited by non-radiative recombination, which leads to phonon emission and, therefore, heat production. The cooling efficiency drops to 17% when the radiative efficiency is 10^{-6} . This result demonstrates that our system works with low radiative efficiencies (e.g. 10^{-6}) while most optical refrigeration systems require radiative efficiency close to unity. Here, with $C = 1$, the thermalisation coefficient does not impact the cooling efficiency. Increasing the concentration factor increases the incident power flux, and since the absorbance is constant, the photogenerated carrier flux also increases. When $C = 100$ (Fig. 5(b)), the 28% maximum cooling efficiency is reached when the radiative efficiency is higher than 10^{-4} and the thermalisation coefficient is higher than $2 \cdot 10^4 \text{ W} \cdot \text{m}^{-2} \cdot \text{K}^{-1}$. Below this value, the electron-phonon interaction becomes too weak and the photogenerated carriers absorb too few phonons before being extracted towards the reservoir, leading to an cooling efficiency decrease. Here, with $C = 100$, the cooling efficiency can be negative. For instance, when $Q = Q_0$ and $\eta_{rad} = 10^{-6}$, $\eta_{cooling} = -15\%$. The incident power flux is such that the carrier extraction does not balance the heating induced by non-radiative recombination. When $C = 10^4$ (Fig. 5(c)), the cooling efficiency can be as low as -42% (e.g. when $Q = Q_0$ and $\eta_{rad} = 10^{-6}$). Remembering that the

superlattice absorbs 45% of the incident sunlight, nearly all the absorbed power is converted into heat. However, the 28% maximum cooling efficiency is reached when the radiative efficiency is higher than 10^{-2} and the thermalisation coefficient is higher than $10^6 \text{ W.m}^{-2}.\text{K}^{-1}$. Here, due to the very high generation rate, the electron-phonon interaction must be strong enough to efficiently extract the carriers. Thus, the cooling efficiency is negative for low thermalisation coefficient. The device can extract a considerable heat flux if the superlattice meets these conditions. With $C = 10^4$, the incident power flux is $1.4 \cdot 10^7 \text{ W.m}^{-2}$ and the cooling power flux (*i.e.* $\eta_{cooling} \times P_{in}$) is then $3.9 \cdot 10^5 \text{ W.m}^{-2}$.

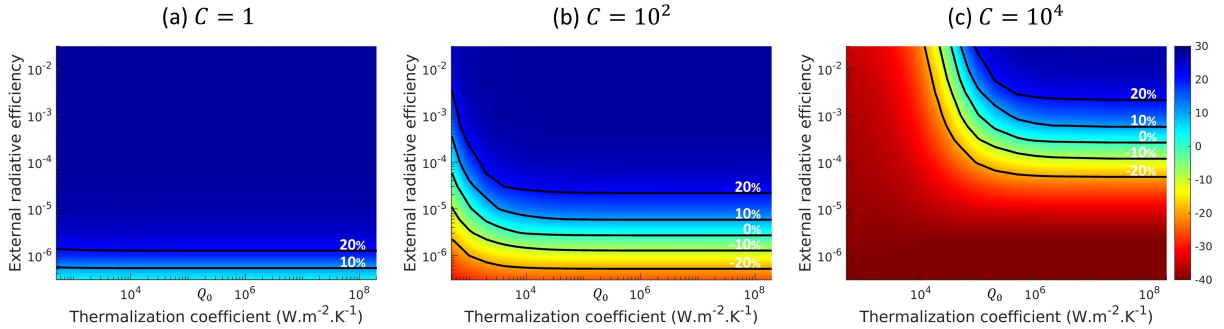


Figure 5: Cooling efficiency $\eta_{cooling}$, in colour scale, versus the external radiative efficiency η_{rad} and the thermalisation coefficient Q for three different concentrations of the solar flux ((a) $C = 1$, (b) $C = 10^2$ and (c) $C = 10^4$). The black lines show the iso-efficiencies of -20%, -10%, 0%, 10% and 20%. Q_0 is the experimental thermalisation coefficient of GaAs multiple quantum wells.

Conclusion

To conclude, we used *ab initio* calculations to investigate a strain-balanced superlattice based on 2D MoS₂ and 2D WSe₂. We found a direct bandgap semiconductor with a bandgap energy of 0.6 eV at the K point of the first Brillouin zone. We evidenced a hybridisation of the electronic states of MoS₂ and WSe₂ close to the valence band edge at the Γ point. This hybridisation should enhance low-energy absorption and emission processes that do not require wave vector conservation, such as impact ionisation. However, the optical absorption is weak below 1.5 eV since the valance and conduction band edges at the K point are

not located in the same TMD. Based on this superlattice, we propose a cooling device working under solar flux thanks to impact ionisation. We consider a type I heterojunction where the small bandgap material is a 50 nm-thick superlattice. By absorbing phonons, the photogenerated carriers can be extracted at higher energy when the superlattice is connected to a larger bandgap bulk MoS₂, leading to its cooling by evaporation. We demonstrate a net cooling efficiency of 28% under sunlight, even considering a low radiative efficiency ($\eta_{rad} = 10^{-6}$). Higher radiative efficiencies enable concentrating the solar flux, without degrading the cooling efficiency to extract more heat from the absorber.

Acknowledgement

The authors thank GELATO ANR project for financial support (ANR-21-CE50-0017).

List of accronyms

2D	Two-dimensional
A	Absorbance
α	Absorption coefficient
C	Concentration factor of the solar flux
c	Speed of light in vacuum
DFT	Density functional theory
E	Photon energy
e-h	Electron-hole
$E_{g_{abs}}$	Bandgap energy of the absorber
$E_{g_{res}}$	Bandgap energy of the reservoir
h	Planck's constant
$J_{extract}$	Carrier flux extracted from the absorber to the reservoir

J_{gen}	Carrier generation flux in the absorber
J_{rec}	Carrier recombination flux in the absorber
k_B	Boltzmann's constant
L	Thickness of the absorber
μ_c	Pseudo-Fermi level of the electrons in the conduction band of the absorber
μ_{res}	Fermi level of the reservoir
μ_v	Pseudo-Fermi level of the holes in the valence band of the absorber
$\Delta\mu$	Fermi level splitting in the absorber
n_{op}	Refractive index of the absorber
η_c	Carnot's efficiency of the device
$\eta_{cooling}$	Cooling efficiency
η_{rad}	External radiative efficiency
Ω_{sun}	Solid angle of the sunlight on earth
P_{in}	Incident power flux density of the light source
$P_{extract}$	Power flux density extracted from the absorber to the reservoir
P_{gen}	Power flux density generated through photon absorption in the absorber
P_{phonon}	Power flux density exchanged between the electronic and phononic baths in the absorber
P_{rec}	Power flux density of the carrier recombination
ϕ_{BB}	Black body radiation
ϕ_{in}	Emission spectrum of the light source
Q	Thermalisation coefficient
Q_0	Experimental thermalisation coefficient of GaAs multiple quantum wells
QY	Quantum yield function
T_{amb}	Room temperature
T_c	Carrier temperature in the absorber
T_{sun}	Sun temperature
TMD	Transition metal dichalcogenides

vdWH Van der Waals heterojunction.

Supporting Information

A derivation of the carrier flux recombination in the absorber, and the corresponding power flux density (Eq. 4) is presented.

References

- (1) Bescond, M.; Dangoisse, G.; Zhu, X.; Salhani, C.; Hirakawa, K. Comprehensive Analysis of Electron Evaporative Cooling in Double-Barrier Semiconductor Heterostructures. *Physical Review Applied* **2022**, *17*, 014001.
- (2) Pringsheim, P. Zwei Bemerkungen über den Unterschied von Lumineszenz- und Temperaturstrahlung. *Zeitschrift für Physik* **1929**, *57*, 739–746.
- (3) Epstein, R. I.; Buchwald, M. I.; Edwards, B. C.; Gosnell, T. R.; Mungan, C. E. Observation of Laser-Induced Fluorescent Cooling of a Solid. *Nature* **1995**, *377*, 500–503.
- (4) Thomas, J.; Maia, L.; Ledemi, Y.; Messaddeq, Y.; Kashyap, R. *Oxide Electronics*; John Wiley & Sons, Ltd, 2021; Chapter 10, pp 353–396.
- (5) Seletskiy, D. V.; Epstein, R.; Sheik-Bahae, M. Laser Cooling in Solids: Advances and Prospects. *Reports on Progress in Physics* **2016**, *79*, 096401.
- (6) Bernardi, M.; Vigil-Fowler, D.; Lischner, J.; Neaton, J. B.; Louie, S. G. Ab Initio Study of Hot Carriers in the First Picosecond after Sunlight Absorption in Silicon. *Physical Review Letters* **2014**, *112*, 257402.
- (7) Jiang, X.; Wang, T.; Xiao, S.; Yan, X.; Cheng, L.; Zhong, Q. Approaching Perfect

- Absorption of Monolayer Molybdenum Disulfide at Visible Wavelengths Using Critical Coupling. *Nanotechnology* **2018**, *29*, 335205.
- (8) Das, S.; Pandey, D.; Thomas, J.; Roy, T. The Role of Graphene and Other 2D Materials in Solar Photovoltaics. *Advanced Materials* **2019**, *31*, 1802722.
- (9) Wang, S.; Cui, X.; Jian, C.; Cheng, H.; Niu, M.; Yu, J.; Yan, J.; Huang, W. Stacking-Engineered Heterostructures in Transition Metal Dichalcogenides. *Advanced Materials* **2021**, 2005735.
- (10) Hao, S.; He, D.; Miao, Q.; Han, X.; Liu, S.; Wang, Y.; Zhao, H. Upconversion Photoluminescence by Charge Transfer in a van Der Waals Trilayer. *Applied Physics Letters* **2019**, *115*, 173102.
- (11) Lai, J.-M.; Sun, Y.-J.; Tan, Q.-H.; Tan, P.-H.; Zhang, J. Laser Cooling of a Lattice Vibration in van Der Waals Semiconductor. *Nano Letters* **2022**, *22*, 7129–7135.
- (12) Qi, P.; Dai, Y.; Luo, Y.; Tao, G.; Zheng, L.; Liu, D.; Zhang, T.; Zhou, J.; Shen, B.; Lin, F. et al. Giant Excitonic Upconverted Emission from Two-Dimensional Semiconductor in Doubly Resonant Plasmonic Nanocavity. *Light: Science & Applications* **2022**, *11*, 176.
- (13) Hua, M.; Decca, R. S. Net Energy Up-Conversion Processes in CdSe/CdS (Core/Shell) Quantum Dots: A Possible Pathway towards Optical Cooling. *Physical Review B* **2022**, *106*, 085421.
- (14) Hanna, M. C.; Nozik, A. J. Solar Conversion Efficiency of Photovoltaic and Photoelectrolysis Cells with Carrier Multiplication Absorbers. *Journal of Applied Physics* **2006**, *100*, 074510.
- (15) Kim, J.-H.; Bergren, M. R.; Park, J. C.; Adhikari, S.; Lorke, M.; Frauenheim, T.; Choe, D.-H.; Kim, B.; Choi, H.; Gregorkiewicz, T. et al. Carrier Multiplication in van

- Der Waals Layered Transition Metal Dichalcogenides. *Nature Communications* **2019**, *10*, 5488.
- (16) Zheng, W.; Bonn, M.; Wang, H. I. Photoconductivity Multiplication in Semiconducting Few-Layer MoTe₂. *Nano Letters* **2020**, *20*, 5807–5813.
- (17) Sheik-Bahae, M.; Epstein, R. I. Can Laser Light Cool Semiconductors? *Physical Review Letters* **2004**, *92*, 247403.
- (18) Zhang, J.; Li, D.; Chen, R.; Xiong, Q. Laser Cooling of a Semiconductor by 40 Kelvin. *Nature* **2013**, *493*, 504–508.
- (19) Yangui, A.; Bescond, M.; Yan, T.; Nagai, N.; Hirakawa, K. Evaporative Electron Cooling in Asymmetric Double Barrier Semiconductor Heterostructures. *Nature Communications* **2019**, *10*, 4504.
- (20) Dalla Valle, P.; Bescond, M.; Michelini, F.; Cavassilas, N. Laser Cooling in Semiconductor Heterojunctions by Extraction of Photogenerated Carriers. *Physical Review Applied* **2023**, *20*, 014066.
- (21) Tsai, C.-Y. Theoretical Model and Simulation of Carrier Heating with Effects of Nonequilibrium Hot Phonons in Semiconductor Photovoltaic Devices. *Progress in Photovoltaics: Research and Applications* **2018**, *26*, 808–824.
- (22) Giteau, M.; de Moustier, E.; Suchet, D.; Esmailpour, H.; Sodabanlu, H.; Watanabe, K.; Collin, S.; Guillemoles, J.-F.; Okada, Y. Identification of Surface and Volume Hot-Carrier Thermalization Mechanisms in Ultrathin GaAs Layers. *Journal of Applied Physics* **2020**, *128*, 193102.
- (23) Green, M. A. Radiative Efficiency of State-of-the-Art Photovoltaic Cells: Radiative Efficiency of Photovoltaic Cells. *Progress in Photovoltaics: Research and Applications* **2012**, *20*, 472–476.

- (24) Spirkel, W.; Ries, H. Luminescence and Efficiency of an Ideal Photovoltaic Cell with Charge Carrier Multiplication. *Physical Review B* **1995**, *52*, 11319–11325.
- (25) Giannozzi, P.; Baroni, S.; Bonini, N.; Calandra, M.; Car, R.; Cavazzoni, C.; Ceresoli, D.; Chiarotti, G. L.; Cococcioni, M.; Dabo, I. et al. QUANTUM ESPRESSO: A Modular and Open-Source Software Project for Quantum Simulations of Materials. *Journal of Physics: Condensed Matter* **2009**, *21*, 395502.
- (26) Giannozzi, P.; Andreussi, O.; Brumme, T.; Bunau, O.; Buongiorno Nardelli, M.; Calandra, M.; Car, R.; Cavazzoni, C.; Ceresoli, D.; Cococcioni, M. et al. Advanced Capabilities for Materials Modelling with Quantum ESPRESSO. *Journal of Physics: Condensed Matter* **2017**, *29*, 465901.
- (27) Perdew, J. P.; Burke, K.; Ernzerhof, M. Generalized Gradient Approximation Made Simple. *Physical review letters* **1996**, *77*, 3865.
- (28) Grimme, S.; Antony, J.; Ehrlich, S.; Krieg, H. A Consistent and Accurate Ab Initio Parametrization of Density Functional Dispersion Correction (DFT-D) for the 94 Elements H-Pu. *The Journal of chemical physics* **2010**, *132*, 154104.
- (29) Hamann, D. R. Optimized Norm-Conserving Vanderbilt Pseudopotentials. *Physical Review B* **2013**, *88*, 085117.
- (30) van Setten, M. J.; Giantomassi, M.; Bousquet, E.; Verstraete, M. J.; Hamann, D. R.; Gonze, X.; Rignanese, G. M. The PseudoDojo: Training and Grading a 85 Element Optimized Norm-Conserving Pseudopotential Table. *Computer Physics Communications* **2018**, *226*, 39–54.
- (31) Monkhorst, H. J.; Pack, J. D. Special Points for Brillouin-zone Integrations. *Physical Review B* **1976**, *13*, 5188–5192.

- (32) Dalla Valle, P.; Cavassilas, N. A van Der Waals Heterojunction Based on Monolayers of MoS₂ and WSe₂ for Overall Solar Water Splitting. *Nanoscale Advances* **2022**, *4*, 2816–2822.
- (33) Bernardi, M.; Palummo, M.; Grossman, J. C. Extraordinary Sunlight Absorption and One Nanometer Thick Photovoltaics Using Two-Dimensional Monolayer Materials. *Nano Letters* **2013**, *13*, 3664–3670.
- (34) Fiore, S.; Luisier, M. Ab Initio Modeling of Thermal Transport through van Der Waals Materials. *Physical Review Materials* **2020**, *4*, 094005.
- (35) Amin, B.; Singh, N.; Schwingenschlögl, U. Heterostructures of Transition Metal Dichalcogenides. *Physical Review B* **2015**, *92*, 075439.
- (36) Zhang, R.; Koutsos, V.; Cheung, R. Elastic Properties of Suspended Multilayer WSe₂. *Applied Physics Letters* **2016**, *108*, 042104.
- (37) Ekins-Daukes, N. J.; Kawaguchi, K.; Zhang, J. Strain-Balanced Criteria for Multiple Quantum Well Structures and Its Signature in X-ray Rocking Curves. *Crystal Growth & Design* **2002**, *2*, 287–292.
- (38) Valle, P. D.; Cavassilas, N. A van Der Waals Heterojunction Based on Monolayers of MoS₂ and WSe₂ for Overall Solar Water Splitting. *Nanoscale Advances* **2022**,
- (39) Akinlami, J. O.; Ashamu, A. O. Optical Properties of GaAs. *Journal of Semiconductors* **2013**, *34*, 032002–5.
- (40) Cavassilas, N.; Aniel, F.; Fishman, G.; Adde, R. Full-Band Matrix Solution of the Boltzmann Transport Equation and Electron Impact Ionization in GaAs. *Solid-State Electronics* **2002**, *46*, 559–566.
- (41) Fountaine, K. T.; Lewerenz, H. J.; Atwater, H. A. Efficiency Limits for Photoelectrochemical Water-Splitting. *Nature Communications* **2016**, *7*, 13706.

TOC Graphic

